Probing the Local pH of Polymer Photoresist Films Using a Two-Color Single Molecule Nanoprobe

Michael D. Mason,* Krishanu Ray, Gerd Pohlers,† James F. Cameron,† and Robert D. Grober

Department of Applied Physics, Yale University, New Haven, Connecticut 06520

Received: September 15, 2003; In Final Form: October 10, 2003

A method has been developed to probe the localized inhomogeneities of acids in thin 193 nm polymer photoresist films using nanomolar concentrations of the pH-sensitive fluorophore Coumarin 6 (C6). C6 exhibits distinct absorption and emission wavelengths for its neutral and protonated forms, allowing the fluorescence for each species to be separated into two distinct detection channels and imaged spatially using two-color confocal microscopy. A two-dimensional thresholding technique was used to distinguish between signal and noise. The ratio (R) of the two intensity channels indicates the degree to which each C6 molecule is protonated, and distributions of these values can be used to describe the relative inhomogeneity in the polymer system for samples with a given average acid concentration. For ensemble measurements of C6 in solution, a single narrow distribution of R-values was obtained. Photoresist film samples prepared from solutions with bulk pH near the pK_a of C6 exhibit broad bimodal distributions centered about the expected mean R-value ($R = 1$). We infer from this result that in these polymer films, at temperatures below the glass transition, proton exchange happens on a very slow time scale. In this case the state of the fluorophore is effectively frozen as either neutral or protonated.

Introduction

Historically, information about the nature of chemical interactions, molecular dynamics, and other physical properties has been obtained from experiments conducted on relatively large ensembles of molecules. While ensemble-averaged experiments provide useful information about average properties, they are less sensitive to provide detailed information about the heterogeneity of each species within the ensemble. Spatial, spectral, and temporal single molecule fluorescence measurements have the specific ability to probe individual species within an ensemble distribution, yielding a range of previously unforeseen characteristics.[1−6] While early single molecule experiments were focused almost exclusively on characterizing the unusual photophysics of the individual fluorescent molecule, more recent work has shifted toward finding applications for single molecules as highly sensitive local nanoprobes.[7] Applications in biology and biochemisty, in particular, have shown great promise.[8−10] For example, new site-specific enzymatic and catalytic processes have been observed that cannot be described using conventional ensemble models and have been attributed to statistical fluctuations in physical properties on the single molecule level.[11] One area where there have been only limited single molecule applications has been in polymer photoresist systems.[12,13] These inherently amorphous materials are used in photolithographic processes, where localized fluctuations in morphology and chemical activity play a key role in the development and quality of the desired patterned nanostructures. Specifically, as lithographic features are pushed to smaller length scales, visualizing the nature and distribution of chemical functionalities at or below the length scale of the features becomes critical.

In the method described in this paper, we dope the pH-sensitive fluorophore Coumarin 6 (C6) at nanomolar levels into a commercial photoresist containing controlled quantities of trifluoroacetic acid (TFA). The use of TFA instead of a photoacid generator (PAG), typically used in photoresist systems, allows us to determine the pH in the solution phase and eliminates the need for prolonged UV exposure, which could photodegrade the dopant fluorophores. The two prototropic forms of C6 exhibit unique fluorescence absorption and emission energies, allowing for their separation into two optical detection pathways in a microscopic imaging technique (Figure 1). The protonation−deprotonation kinetics of the C6−photoresist system can also be investigated by comparing the pH-dependent single molecule distributions for samples at varying acid concentrations. Intensity information is extracted directly from

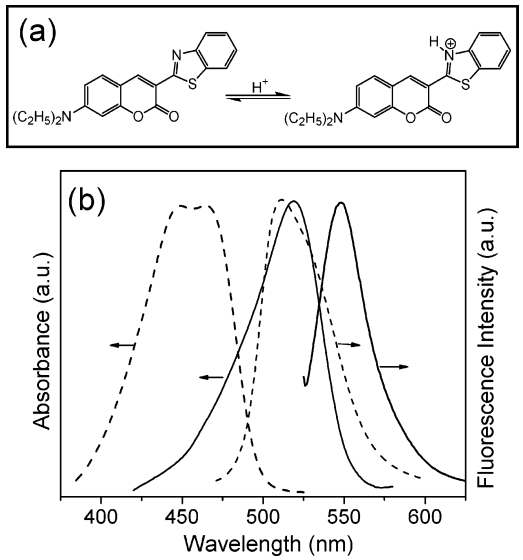

Figure 1. (a) Structure of neutral and protonated forms of Coumarin 6 (C6). (b) Absorption and fluorescence spectra of C6 (- - -) and $C6^+$ (—) at micromolar concentration in a Silsesquioxane polymer photoresist film.

* To whom correspondence should be addressed.
† Shipley Company, Marlborough, MA 01752.

10.1021/jp036745j CCC: $25.00
Published on Web 11/27/2003

the image data, and nearly all points corresponding to emission from individual fluorophores are retained, generating meaningful histograms from a small number of fluorophores (and images) including those which are typically excluded due to inadequate signal.

Experimental Section

Commercially available C6 (Aldrich Inc.) was recrystallized from CH_3OH/CH_2Cl_2 to reduce impurity levels.[14] Silsesquioxane polymers $(SiO_2-R_1)_n-(SiO_2-R_2)_m$ (Shipley Inc.) were synthesized by acid-catalyzed condensation polymerization according to literature procedures.[15] The number-average molecular weights (M_n) are in the 3000−10 000 range, as determined by gel permeation chromatography calibrated with polystyrene standards. All polymers used in this study were characterized by ^1H, ^{29}Si, and ^{13}C NMR, HPLC, FT-IR, and MALDI-TOF spectroscopy as well as thermal and elemental analyses. Solution samples with micromolar concentrations of C6 in polymer photoresist, with increasing acid concentrations, were prepared on welled glass slides capped with a coverslip. Single molecule film samples were prepared on a standard glass coverslip by spin-casting solutions of the polymer photoresist, 10^{-9} M C6, and spectroscopic grade trifluoroacetic acid (TFA) in diglyme (Aldrich Inc). The concentration of TFA in a series of solutions was adjusted such that the pH varied from neutral (∼6.0) to acidic (∼1.0) prior to spinning. For simplicity, we refer to solutions where no acid was added as "neutral", but were actually found to be slightly acidic (pH ∼6.0), possibly due to some intrinsic free acid in the polymer solutions. Utmost care was taken during sample preparation to minimize the possible introduction of environmental contaminants (fluorescence impurities). Films were prepared with pH values of 6.0, 5.5, 4.5, 3.5 3.0, 2.5, and 1.0, which were verified by traditional titration methods. The resulting films had thicknesses of ∼100 nm as verified by profilometry.

Emission from C6 molecules was imaged in two channels using a laser scanning confocal microscope (LSCM) with a 100× high numerical aperture (Nikon, 1.25 NA) oil-immersion objective. Simultaneous excitation of both the neutral and protonated species of C6 was accomplished using the 457 nm line of an Ar^+ laser (Coherent) and a 532 nm diode-pumped solid state laser (Figure 2). The separate excitation beams were spatially filtered by passing each through a 25 μm pinhole. Each beam was passed through a quarter wave plate, resulting in circularly polarized light for uniform excitation of the fluorophores in the sample plane. The individual beams were recollimated and their beam widths adjusted, using a Gaussian beam expander in one path, such that the wavelength-dependent excitation profile at the sample was the same for each. The diffraction limited spot size, as well as relative alignment, for each source was verified by imaging the change in reflectance over a standard of latex spheres (<50 nm) on glass. This procedure allowed us to monitor the alignment of both beams, as well as provided a way to carefully control the power density at each wavelength. The total collected fluorescence was split using a 50/50 nonpolarizing broadband cube beam splitter (Newport Optics) and directed into the two detection channels. A 500 ± 20 nm band-pass filter and 560 nm long-pass filter (Chroma Inc.) were used in the neutral and protonated detection channels, respectively, to remove the contributions due to other species as well as stray laser light. Furthermore, a 600 nm short-pass filter was placed in front of the cube beam splitter excluding the red/near-IR emission known to exist in these polymer systems. Finally, the collected light in each channel was imaged

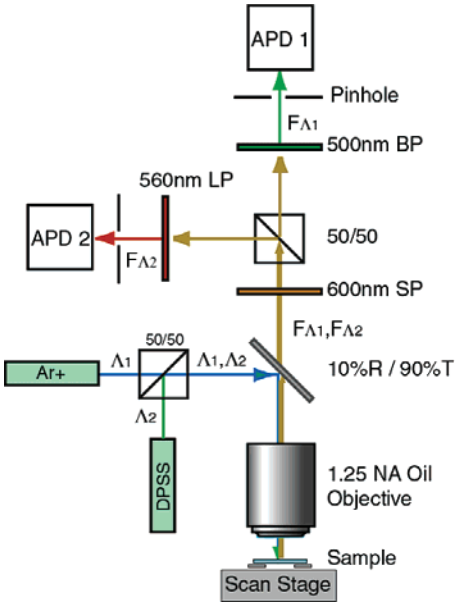

Figure 2. Schematic representation of the simultaneous two-color scanning confocal microscope setup used in the experiments described in the text.

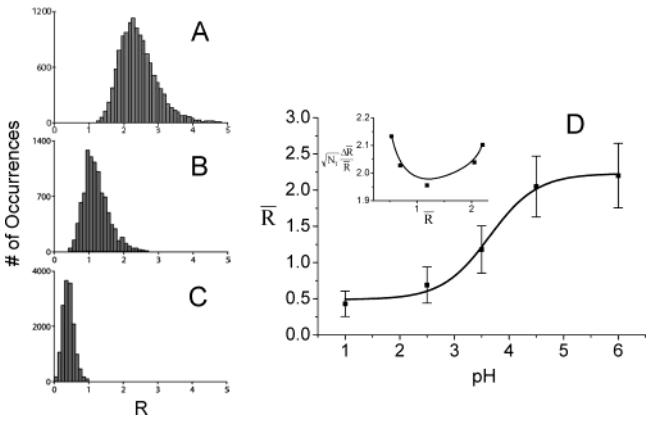

Figure 3. Histogram of the ratio $R = I_N/I_P$ obtained from the images of C6 (5×10^{-6} M) in diglyme at pH values of 6 (A), 3.5 (B), and 1 (C). (D) The mean values of R extracted from the histogram data vs pH for a series of samples with increasing acid concentration. The inset of panel (D) shows the plot of $\sqrt{N_T}\,\Delta\bar{R}/\bar{R}$ vs $\bar{R}$ for the experimental data and theoretical values predicted by eq 12.

onto a 50 μm pinhole and directed onto an avalanche photodiode (APD) (EG&G). To provide sufficient signal-to-noise ratio, 10 μW laser excitation was used, generating power densities of ∼5 kW/cm^2 at the sample. Intensity data for both the solution and polymer film samples were obtained in image format. Integration times of 10 ms per pixel were used to obtain 128 × 128 pixel raster scanned 10 × 10 μm images.

Results and Discussion

Solution samples containing micromolar concentrations of C6 were imaged in order to determine the ensemble behavior of the fluorophore in this system, as well as to set a baseline for our data analysis scheme. As expected, the images (not shown) exhibited no spatial contrast due to the free diffusion through the focal volume and the relatively high local concentration of the fluorophore. Histograms of the ratio (R) of the intensities in the neutral and protonated channels (I_N, I_P) were obtained for each sample as shown in Figure 3A−C. The mean R-value for each histogram versus pH is plotted in Figure 3D, where the error bars shown represent the width ($\pm\sigma$) of the distribution.

A simple two-state titration model can be obtained from the rate equations describing the protonation and deprotonation kinetics of neutral (N) and protonated (P) C6 respectively:

$$\mathrm{N} + \mathrm{H} \underset{k_{-1}}{\overset{k_1}{\rightleftharpoons}} \mathrm{P} \tag{1}$$

$$\frac{dN}{dt} = k_{-1}P - k_1 NH \tag{2}$$

$$\frac{dP}{dt} = -k_{-1}P + k_1 NH \tag{3}$$

At equilibrium, where $K_a = [\mathrm{N}][\mathrm{H}]/[\mathrm{P}]$, and $N + P = C_T$ (the total number of C6 molecules measured), the above rate equations can be simplified to

$$N = \frac{K_a}{K_a + H} C_T \tag{4}$$

$$P = \frac{H}{K_a + H} C_T \tag{5}$$

The measured optical signal in each channel can be represented by the following equations:

$$I_N = g_N N + g_P \gamma_P P \tag{6}$$

$$I_P = g_N \gamma_N N + g_P P \tag{7}$$

where g_N and g_P contain the quantum efficiency of the fluorophore, the collection efficiency of the microscope, and the quantum efficiency of the APD, for the neutral and protonated species, respectively. The parameters γ_N and γ_P are terms describing the leakage (spectral overlap) of the neutral emission into the protonated channel and vice versa and have typical values of 15% and 0.01%, respectively. Substituting eqs 4 and 5 into eqs 6 and 7 yields the following functional form:

$$\mathrm{pH} = \mathrm{p}K_a + \log\left(\frac{g_P}{g_N}\bar{R}_{max}\right) + \log\left(\frac{\bar{R} - \bar{R}_{min}}{\bar{R}_{max} - \bar{R}}\right) \tag{8}$$

where $\bar{R}$ is the mean R obtained from a histogram of I_N/I_P values, $\bar{R}_{min}$ represents the leakage between collection channels, and $\bar{R}_{max}$ is the maximum value R for the two-state titration curve. When eq 8 was fit to the solution data (Figure 3D), the following values were obtained: $\bar{R}_{min} = 0.38$, $\bar{R}_{max} = 2.3$, and $\mathrm{p}K_a = 3.3$. The available literature value for the pK_a of C6 is 1.6 in 50:50 CH_3OH/H_2O.[14] The value of 3.3 obtained from the model fit is reasonable considering that a change in solvent, from CH_3OH/H_2O to aprotic diglyme, could easily result in an increase of approximately 1−2 pK_a unit.[16]

To interpret the results, it is important to consider the effects of noise due to the photon-counting statistics of our measurement. The mean normalized standard deviation, $\Delta\bar{R}/\bar{R}$, can be described by first considering the mean R ($\bar{R}$) as the ratio of two random variables (I_N, I_P) with fluctuating components (δI_N, δI_p), respectively:

$$\bar{R} = \frac{I_N + \delta I_N}{I_P + \delta I_P} \tag{9}$$

which can be closely approximated as

$$\bar{R} \cong \left(1 + \frac{\delta I_N}{I_N} - \frac{\delta I_P}{I_P}\right) \tag{10}$$

The standard deviation of R can be written as

$$\Delta\bar{R} = \bar{R}\sqrt{\left(\frac{\delta I_N}{I_N}\right)^2 + \left(\frac{\delta I_P}{I_P}\right)^2} \tag{11}$$

where δI_N and δI_p for a Poisson process are $\sqrt{I_N}$ and $\sqrt{I_P}$, respectively. For dependent fluctuations there is an additional cross-correlation term in eq 11, which for relevant values of I_N and I_P, adjusts the standard deviation by $\pm <3\%$, and is generally omitted. By rearranging and substituting $N_T = I_N + I_P$, we obtain the following relationship for the mean normalized standard deviation in $\bar{R}$:

$$\frac{\Delta\bar{R}}{\bar{R}} = \sqrt{\frac{1 + \bar{R}}{N_T}}\sqrt{1 + \frac{1}{\bar{R}}} \tag{12}$$

The quantum efficiency of protonated C6 is approximately half that of neutral C6;[17] therefore, as the pH of the film is decreased, we expect N_T to decrease and $\Delta\bar{R}/\bar{R}$ to increase. This behavior has been previously reported for the pH-sensitive dye SNARF-1.[18] A plot of $\sqrt{N_T}(\Delta\bar{R}/\bar{R})$ ($\Delta\bar{R}/\bar{R}$ normalized by multiplying by $\sqrt{N_T}$) versus $\bar{R}$ values obtained from the mean, standard deviation, and mean total photon counts (N_T) of the histogram data for the series of solution samples and that obtained from eq 12 are shown in the inset in Figure 3D. They are in good agreement, exhibiting a minimum value at the equivalence point ($\bar{R} = 1$), as predicted by eq 12.

In Figure 4 representative two-color confocal images of C6 (1 nM) in photoresist with varying acid concentrations are shown. Emission of the neutral species (Figure 4A,C,E) and the protonated species (Figure 4B,D,F) were obtained simultaneously, and are shown for three different acid concentrations (pH 6, 3.5, and 1, respectively). In all, films were prepared from seven different solutions with pH values of 1, 2.5, 3, 3.5, 4.5, 5.5, and 6 (no acid added).

It is immediately evident from Figure 4 that photobleaching was prevalent in the samples containing little or no acid, resulting in a few well-resolved circular diffraction limited spots usually associated with the presence of individual fluorophores in confocal images. We found this to be true regardless of excitation power. This may have been due to an increased sensitivity to photobleaching caused by the oxide-rich composition of the polymer film system which was slightly hindered at higher acid concentrations.[19]

The typical approach for analyzing two-channel single molecule image data has been to fit the bright diffraction limited spots in an image, corresponding to the fluorophore position, to an appropriate optical response function and to extract the fitted peak heights. Photobleaching and blinking was prevalent in the photoresist film samples, making it difficult to apply typical Gaussian peak fitting routines to extract emission intensities or to re-image the same area. We have implemented the following statistical thresholding technique in order to use the data at each point in the image rather than relying on a more complicated image analysis. First, the mean background level of each image was determined. This was accomplished by calculating the mean intensity over all points in the image and then excluding those pixels with values greater than the mean plus two standard deviations (i.e., the points with real signal) and recalculating a new background level. This was repeated iteratively until the value for the new background level converged, corresponding to the noise level. Because most points in the image are due to background, and we want to extract only those points due to real signal, a threshold was applied to

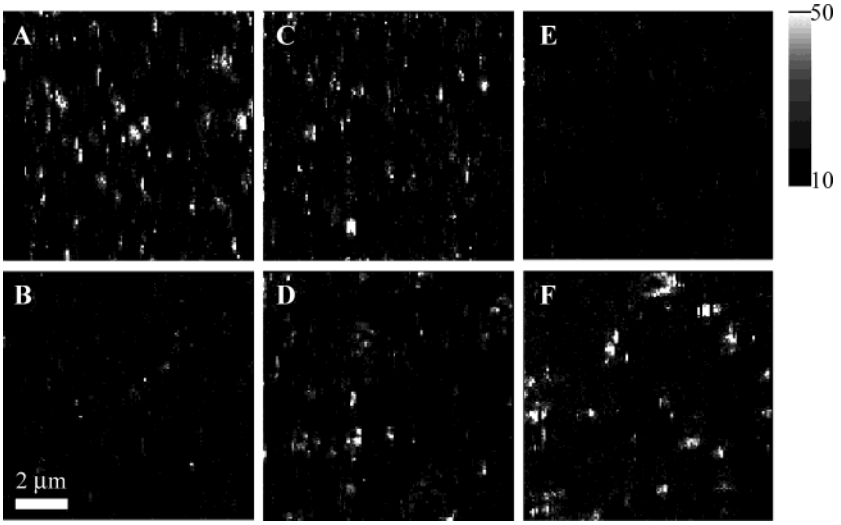

Figure 4. Fluorescence images of C6 molecules in 193 nm photoresist films at different pH values, recorded in two detection channels simultaneously. (A), (C), and (E) correspond to emission from a 480−520 nm spectral range, and (B), (D), and (F) correspond to a spectral range around 560−600 nm. Image sets (A) and (B), (C) and (D), and (E) and (F) correspond to film samples prepared from a solution at pH 6, 3.5, and 1, respectively.

each image at the background mean plus three standard deviations from the mean. If a point, in either image channel, was above this threshold, the corresponding points in both images were kept. In this way, points which correspond to a single molecule which has blinked "off" or photobleached are not used as they generate no fluorescence signal and, therefore, have no statistical impact. This corresponds to a ~99% confidence level that the retained points, in each image, are due to real signal and resulted in the retention of approximately 10% of the total number of points. The retained points were used to calculate the ratio (R) of the intensity in the neutral channel to the intensity in the protonated channel (I_N/I_P). These data are shown as R-value histograms along the y-axis of Figure 5A−C for samples with three different acid concentrations.

If the intensity of a pixel was above the threshold, but was only due to a large statistical fluctuation in the noise, and the corresponding pixel in the other channel happened to fluctuate below the background, then the resulting value of R would be either very small or very large. If a significant number of retained pixels fall into this category (where the signal-to-noise ratio is small), then a resulting histogram of R-values would not accurately represent the single molecule data. To minimize this effect, the total number of photons counted (N_T) for each pair of pixels was also considered. Two-dimensional histograms consisting of the R-values (y-axis) and the N_T-values (x-axis) were generated as shown in Figure 5A−C, where the number of occurrences are shown as the color-scaled contour lines. The resulting distributions for high and low pH values clearly exhibit a dual population behavior, with one population occurring at higher values of N_T. At pH values near the equivalence point (pK_a) of C6, the bimodal populations occur at nearly the same value of N_T. When a threshold is applied to each two-dimensional histogram at a value of N_T equal to the sum of the individual image thresholds ($I_N + 3\sqrt{I_N} + I_P + 3\sqrt{I_P}$), shown as the dashed lines in Figure 5A−C, and the remaining R-values are compiled, the R-value histograms shown in Figure 5D−F are obtained. As previously mentioned, due to a decrease in quantum efficiency the total number of photons, and therefore the applied threshold, decreases slightly going from neutral to protonated samples. The high (pH 6) and low (pH 1) histograms exhibit predominately single populations with $\bar{R}$ values around 1.8 and 0.5, respectively. The small peak in Figure 5D around $\bar{R} = 0.5$ is likely due to leakage of the neutral emission into the protonated channel. The samples at pH 3.5, however, have two distinct populations: with values around 1.5 and 0.5, with $\bar{R}$ around 1.

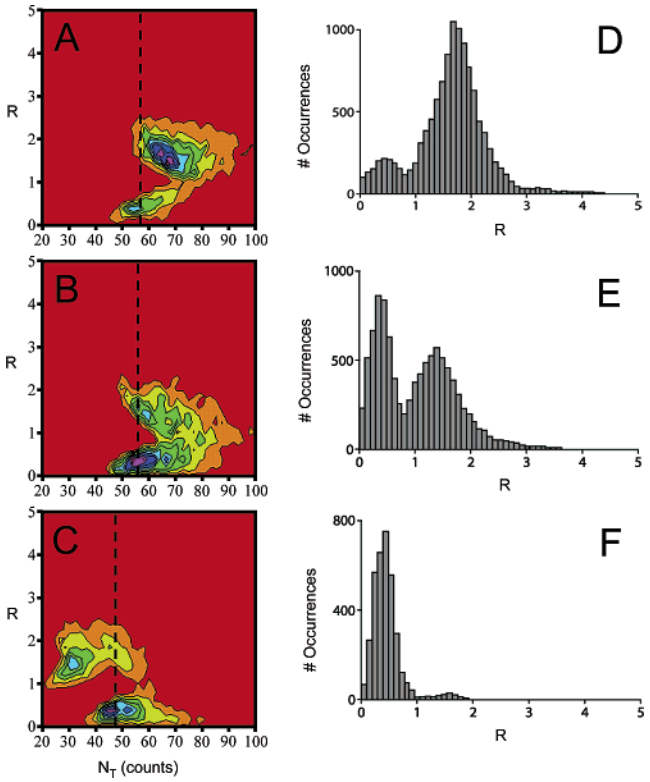

Figure 5. Two-dimensional histogram of R vs total counts (N_T) at pH 6 (A), 3.5 (B), and 1 (C), where the number of occurrences is shown using a false-color scale. The dashed lines represent the applied threshold for each data set (N_T = 58, 56,and 49). The histograms resulting from 2-D thresholding for samples at pH 6, 3.5, and 1 are shown in (D), (E) and (F), respectively.

The $\bar{R}$ values, resulting from the thresholding technique above, for a range of samples with increasing pH are shown in Figure 6. The data have been fit to eq 8, with the resulting fit parameters: $\bar{R}_{min} = 0.4$, $\bar{R}_{max} = 1.9$, p$K_a = 3.7$. While the general trend is an increase in $\Delta\bar{R}/\bar{R}$ at higher pH values, a maximum is observed at values around the pK_a point (pH 3.5), as shown in the plot of $\sqrt{N_T}(\Delta\bar{R}/\bar{R})$ versus $\bar{R}$ (Figure 6). This

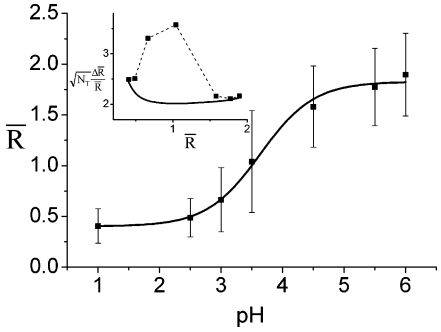

Figure 6. $\bar{R}$ vs pH curve of C6 in 193 nm photoresist film deduced from the single molecule image data. The inset of panel D shows a plot of $\sqrt{N_T}\,\Delta\bar{R}/\bar{R}$ vs $\bar{R}$ extracted from the single molecule images compared with the expected values.

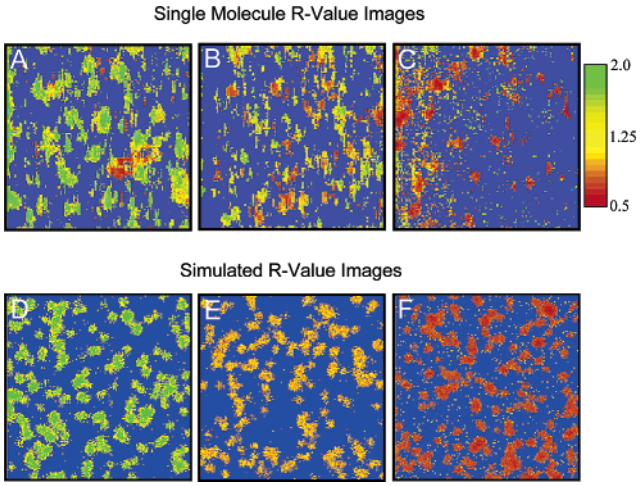

Figure 7. False-color scaled *R*-value images of C6 molecules in 193 nm photoresist films with bulk pH values of 6 (A), 3.5 (B), and 1 (C). Corresponding *R*-value images simulated using the experimental parameters for pH ($\bar{R}$), average signal, and background levels assuming fast proton exchange dynamics and no photobleaching or fluorescence intermittency are shown in (D), (E), and (F).

behavior was not observed in the solution studies, and deviates from the expected minimum in $\sqrt{N_T}(\Delta\bar{R}/\bar{R})$ predicted by eq 12.

The bimodal behavior (Figure 5E), with a minimum at $R = 1$, seems to suggest that in the polymer films the protonation state of C6, especially near pK_a, is spatially inhomogeneous. If we keep only those points used in the histograms, but retain all the spatial information, the extent to which the pH of the C6 varies within the films can be observed in image format. This is shown using a false color scale in Figure 7 for three pH values (6, 3.5, and 1), where all blue points in the image correspond to those, which were excluded by the two-dimensional threshold. The samples which contained no acid or those which are fully protonated (Figure 7A and 7C, respectively) generally exhibit features with only very small fluctuations in color, suggesting that the fluctuations in the protonation state of C6 are not observed. For samples with acid concentrations near the equivalence point of C6, we see a range of *R*-values, as indicated by the histograms, with a majority of the features appearing as neutral or protonated but only a few as something in between (yellow-orange). This bimodal behavior is only observable when nanomolar concentrations of C6 (single molecule level) are present in the film sample. The presence of single molecule features in the images indicates that the observed deviations from the expected intermediate value ($R = 1$) are not simply due to noise fluctuations between the two detection channels.

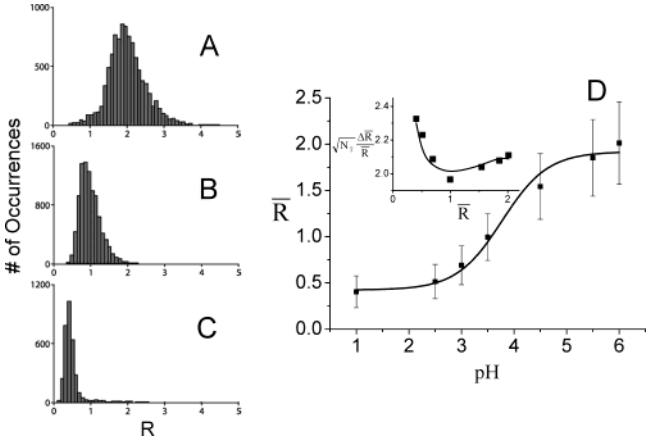

Figure 8. Histogram of the ratio $R = I_N/I_P$ deduced from the simulated image data of C6 where the pH values are 6 (A), 3.5 (B), and 1 (C). (D) $\bar{R}$ vs pH curve from the simulated data. The model is described in detail in the text. The inset of panel D shows a plot of $\sqrt{N_T}\,\Delta\bar{R}/\bar{R}$ vs $\bar{R}$ extracted from the simulated images compared with the predicted values.

Rather, it suggests that each C6 is frozen in either its protonated or neutral state.

As a way of testing our understanding of how the C6 molecules behave in these systems, a series of simulated single molecule images were generated. The average peak emission intensities and background levels from the real data were used as parameters in the model. Diffraction limited Gaussian features with a normal distribution of random peak intensities were generated, where no photobleaching or blinking[20] of the fluorophore occurred. The distribution of acid within the film was made uniform, resulting in the same value of *R* for each fluorophore, and ensuring that all noise was due only to photon fluctuations. Furthermore, this model assumes that near the equivalence point the free proton hops back and forth between C6 and the matrix rapidly, and frequently, relative to the 10 ms integration period. This means that C6 appears as a superposition of its neutral and protonated forms with equivalent intensity in each detection channel resulting in $R = 1$. To account for statistical fluctuations of the photon-counting experiment, Poisson distributed noise was added to each pixel in the simulated images. Finally, the two-dimensional threshold was applied to the simulated images (Figure 7D−F) and *R*-value histograms were generated as depicted in Figure 8A−C. The resulting histograms consist of single populations, where the decrease in *R* going toward lower pH levels is well described by eq 8, as shown in Figure 8D, with fit parameters $\bar{R}_{max} = 1.9$, $\bar{R}_{min} = 0.4$, and p$K_a = 3.6$, consistent with the single molecule data. $\sqrt{N_T}(\Delta\bar{R}/\bar{R})$, shown as the inset in Figure 8D, behaves according to eq 12, with a local minimum at $R = 1$, and is similar to that observed in the solution samples. The fact that our simulation is in good agreement with the solution data and the high and low pH single molecule data strongly suggests that the bimodal distribution observed in the single molecule data near pK_a is a real property of the fluorophore/film system and not an artifact of our thresholding technique.

The unexpected deviation in $\sqrt{N_T}(\Delta\bar{R}/\bar{R})$ from the ideal (simulated) behavior can easily be seen by comparing the two raw data sets for each channel. In Figure 9 scatter plots of the intensity in the neutral (I_N) channel versus protonated (I_P) channel are shown for a series of simulated (red) and real single molecule data (black). For these data, no thresholding has been applied and every point in the images, including background, has been included. For the pH 1 and pH 6 samples (Figure 9A,C)

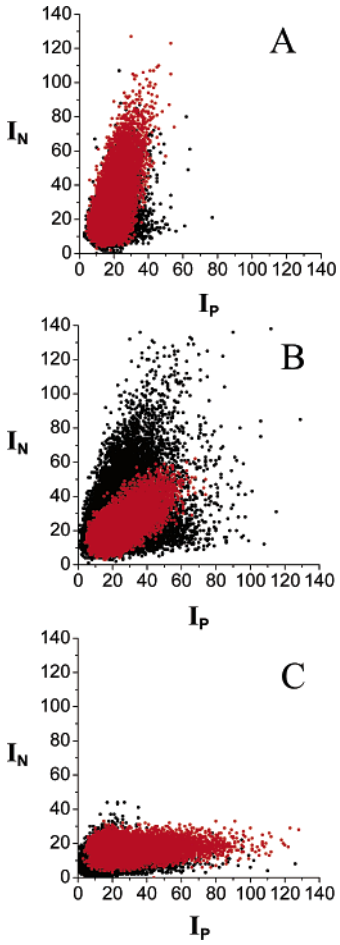

Figure 9. Scatter plots (I_N vs I_P) of all data points taken from one set of single molecule images prior to thresholding. Black dots correspond to the experimental single molecule data, whereas red dots are taken from a simulated image set. Panels A, B, and C are obtained at pH 6, 3.5, and 1, respectively.

the scatter patterns of the simulated and real data nearly overlap. Here the leakage term (γ_P) of eq 6, or $\bar{R}_{min}$ in eq 8, is apparent as the degree to which the scatter plots in Figure 9A deviate from vertical. At the equivalence point (Figure 9B) the single molecule scatter pattern is very broad and deviates dramatically from the expected (simulated) behavior shown in red.

In solution near pK_a, the proton exchange dynamics[21] are very fast relative to the measurement period (10 ms), and each fluorophore appears as a superposition of its neutral and protonated states (Figure 3B). This results in nearly equivalent signals in each detection channel (up to the statistical fluctuations) and a narrow *R*-value distribution centered at $R = 1$ (Figure 3B). When the solution is used to cast a film, the picture may become quite different. As the solvent quickly evaporates, the film becomes more viscous, which may dramatically alter the proton exchange rates as the matrix is less able to reorganize itself to accommodate the exchange of the proton from the fluorophore to the matrix and vice versa. An equivalent statement might be to say that the barrier for proton exchange (ΔG) is much larger than k_BT, reducing the likelihood, and therefore the frequency, of the transition such that it occurs on time scales longer than our 10 ms integration period. This has the effect of "freezing out" the positions of the proton, leaving the C6 in either its protonated or neutral state. This implies that, near the pK_a of C6, the apparent fluctuations in the state of the individual fluorophores, observed in the *R*-images of Figure 7B, may not be indicative of local variation in the pH of the film. Rather, the image can be interpreted as a snapshot of the state of each C6 molecule at the moment the film was cast and the solvent evaporated.

Conclusions

The application of two-color scanning confocal microscopy to the spatially resolved detection of pH-sensitive fluorophore C6 has been reported. The two optically separable prototropic forms of C6 were imaged in two detection channels, and the ratio (*R*) between the two channels was calculated at each image pixel. A simple analytical thresholding technique has been applied to distinguish between those image pixels due to noise and those due to signal. The large number of remaining points resulted in histograms that very accurately represent the distribution of *R*-values within the polymer film system. Films prepared from solutions with acid concentrations near the pK_a of C6 exhibit bimodal distributions, of the neutral and protonated species of C6, as observed in the *R*-value histograms. This indicates that the normally fast proton exchange dynamics are "frozen out" in the film system. This suggests that temperature-dependent studies could provide valuable insight into the protonation−deprotonation kinetics of these systems. This technique further demonstrates the sensitivity of the single molecule to its local environment, as well as the potential for generating information about the photophysical and photochemical properties of the fluorophore−film system, using a relatively simple statistical analysis. In particular, this technique could be used to visualize the state and distribution of photogenerated acids along exposed photoresist features, where the local acid concentrations are expected to vary (or decrease sharply), yielding valuable information about lithographically relevant properties such as acid diffusion and edge roughness.

Acknowledgment. This material is based on work supported by Semiconductor Research Corporation and the National Science Foundation under Grant 0211422.

References and Notes

(1) Macklin, J. J.; Trautman, J. K.; Harris, T. D.; Brus, L. E. *Science* **1996**, *272*, 255.
(2) Basche, T.; Moerner, W. E. *Nature* **1992**, *355*, 335.
(3) Xie, X. S.; Dunn, R. C. *Science* **1994**, *265*, 361.
(4) Ambrose, W. P.; Goodwin, P. M.; Martin, J. C.; Keller, R. A. *Phys. Rev. Lett.* **1994**, *72*, 160.
(5) Weston, K. D.; Buratto, S. K. *J. Phys. Chem. A* **1998**, *102*, 3635.
(6) Vanden Bout, D. A.; Yip, W. T.; Hu, D. H.; Fu, D. K.; Swager, T. M.; Barbara, P. F. *Science* **1997**, *277*, 1074.
(7) Moerner, W. E. *Science* **1994**, *265*, 46.
(8) Weiss, S. *Science* **1999**, *283*, 1676.
(9) Seisesgerber, G.; Ried, M. U.; Endress, T.; Buning, H.; Hallek, M.; Brauchle, C. *Science* **2001**, *294*, 1929.
(10) Ha, T. J.; Zhuang, X.; Kim, H. D.; Orr, J. O.; Williamson, J. R.; Chu, S. *Proc. Natl. Acad. Sci. U.S.A.* **1999**, *96*, 9077.
(11) Lu, H. P.; Xun, L. Y.; Xie, X. S. *Science* **1998**, *282*, 1877.
(12) Deschenes, L. A.; Vanden Bout, D. A. *Science* **2001**, *292*, 255.
(13) Feke, G. D.; Grober, R. D.; Pohlers, G.; Moore, K.; Cameron J. F. *Anal. Chem.* **2001**, *73*, 3472.
(14) Corrant, S.; Hahn, P.; Pohlers, G.; Connolly, T. J.; Scaiano, J. C.; Fornes, V.; Garcia, H. *J. Phys. Chem. B* **1998**, *102*, 5852.
(15) (a) Crivello, J. V.; Mao, Z. *Chem. Mater.* **1997**, *9*, 1554. (b) Fasce, D. P.; Williams, R. J. J.; Méchin, F.; Pascault, J. P.; Llauro, M. F.; Pétiaud, R. *Macromolecules* **1999**, *32*, 4757.
(16) Sober, H. A. *Handbook of Biochemistry*; The Chemical Rubber Company: Cleveland, OH, 1968.
(17) Jones, G.; Jimenez, J. A. C. *J. Photochem. Photobiol. B* **2001**, *65*, 5.
(18) Brasselet, S.; Moerner, W. E. *Single Mol.* **2000**, *1*, 17.
(19) Xie, X. S.; Trautman, J. K. *Annu. Rev. Phys. Chem.* **1998**, *49*, 441.
(20) Dickson, R. M.; Cubitt, A. B.; Tsien, R. Y.; Moerner, W. E. *Nature* **1997**, *388*, 355.
(21) Peters, K. S.; Kim, G. *J. Phys. Chem. A* **2001**, *105*, 4177.